

Updated Determination of the Solar Neutrino Fluxes from Solar Neutrino Data

Johannes Bergström,^a M. C. Gonzalez-Garcia,^{a,b,c} Michele Maltoni,^d Carlos Peña-Garay,^e Aldo M. Serenelli,^f Ningqiang Song,^c

^a*Departament d'Estructura i Constituents de la Matèria and Institut de Ciències del Cosmos, Universitat de Barcelona, Diagonal 647, E-08028 Barcelona, Spain*

^b*Institució Catalana de Recerca i Estudis Avançats (ICREA)*

^c*C.N. Yang Institute for Theoretical Physics, State University of New York at Stony Brook, Stony Brook, NY 11794-3840, USA*

^d*Instituto de Física Teórica UAM/CSIC, Calle de Nicolás Cabrera 13–15, Universidad Autónoma de Madrid, Cantoblanco, E-28049 Madrid, Spain*

^e*Instituto de Física Corpuscular (IFIC), CSIC & Universitat de Valencia Calle Catedrático José Beltrán, 2, E-46090 Paterna, Valencia, Spain*

^f*Institut de Ciències de l'Espai (ICE-CSIC/IEEC), Campus UAB, Carrer de Can Magrans s/n, 08193 Cerdanyola del Vallès, Spain*

E-mail: bergstrom@ecm.ub.edu, maria.gonzalez-garcia@stonybrook.edu,
michele.maltoni@csic.es, penya@ific.uv.es, aldos@ice.csic.es,
ningqiang.song@stonybrook.edu

ABSTRACT: We present an update of the determination of the solar neutrino fluxes from a global analysis of the solar and terrestrial neutrino data in the framework of three-neutrino mixing. Using a Bayesian analysis we reconstruct the posterior probability distribution function for the eight normalization parameters of the solar neutrino fluxes plus the relevant masses and mixing, with and without imposing the luminosity constraint. We then use these results to compare the description provided by different Standard Solar Models. Our results show that, at present, both models with low and high metallicity can describe the data with equivalent statistical agreement. We also argue that even with the present experimental precision the solar neutrino data have the potential to improve the accuracy of the solar model predictions.

KEYWORDS: solar neutrinos

Contents

1	Introduction	1
2	Analysis framework	3
3	Determination of solar neutrino fluxes	6
4	Comparison with the Standard Solar Models	9
5	Generalizing/strengthening the solar models	11
6	Summary and outlook	13
A	Borexino	14

1 Introduction

The Sun generates power through nuclear fusion, the basic energy source being the conversion of four protons into an alpha particle, two positrons and two neutrinos. As early as 1939 [1], Bethe identified two different mechanisms by which such overall process could take place, now known as the pp-chain and the CNO-cycle [2]. In the pp-chain, fusion reactions among elements lighter than $A = 8$ produce a characteristic set of neutrino fluxes, whose spectral energy shapes are known but whose normalization must be calculated with a detailed solar model. In the CNO-cycle the abundance of ^{12}C plus ^{13}N acts as a catalyst, while the ^{13}N and ^{15}O beta decays provide the primary source of neutrinos.

In order to precisely determine the rates of the different reactions in the two chains and to obtain the final neutrino fluxes and their energy spectrum, a detailed modeling of the Sun is needed. Standard Solar Models (SSMs) [3–10] derive the properties of the present Sun by following its evolution after entering the main sequence. The models use as inputs a set of observational parameters (the present surface abundances of heavy elements and surface luminosity of the Sun, as well as its age, radius and mass) and rely on some basic assumptions: spherical symmetry, hydrostatic equilibrium, initial homogeneous composition, evolution at constant mass. Over the past five decades the solar models were steadily refined with the inclusion of more precise observational and experimental information about the input parameters (such as nuclear reaction rates and the surface abundances of different elements), with more accurate calculations of constituent quantities (such as radiative opacity and equation of state), the inclusion of new physical effects (such as element diffusion), and the development of faster computers and more precise stellar evolution codes.

The produced neutrinos, given their weak interactions, can exit the Sun practically unaffected, and therefore enable us to see into the solar interior and verify directly our understanding of the Sun [11]. This was the goal of the original solar neutrino experiments, which was somewhat diverted by the appearance of the so-called “solar neutrino problem” [12, 13]. Such problem has now been fully solved through the modification of the Standard Model with inclusion of neutrino masses and mixing, which allow for flavor transition of the neutrino from production to detection [14–17] and for non-trivial effects (the so called LMA-MSW flavor transitions) when crossing dense regions of matter. The upcoming of the real-time experiments Super-Kamiokande and SNO and the independent determination of the flavor oscillation probabilities using reactor antineutrinos at KamLAND has allowed for the precise determination of the neutrino parameters (masses and mixing) responsible for these flavor transitions.

In parallel to the increased precision in our understanding of neutrino propagation, a new puzzle has emerged in the consistency of SSMs [18]. SSMs built in the 1990’s were very successful in predicting other observations. In particular, quantities measured by helioseismology such as the radial distributions of sound speed and density [5–8] showed good agreement with the predictions of the SSM calculations and provided accurate information on the solar interior. A key element to this agreement is the input value of the abundances of heavy elements on the surface of the Sun [19]. However, since 2004 new determinations of these abundances have become available, pointing towards substantially lower values [20, 21]. The SSMs based on such lower metallicities fail at explaining the helioseismic observations [18].

So far there has not been a successful solution of this puzzle as changes in the Sun modeling do not seem able to account for this discrepancy [10, 22, 23]. Thus the situation is that, at present, there is no fully consistent SSM. This led to the construction of two different sets of SSMs, one based on the older solar abundances [19] implying high metallicity, and one assuming lower metallicity as inferred from more recent determinations of the solar abundances [20, 21]. In Ref. [10, 24] the solar fluxes corresponding to such two models were detailed, based on updated versions of the solar model calculations presented in Ref. [8].

In Ref. [25] we performed a solar model independent analysis of the solar and terrestrial neutrino data in the framework of three-neutrino masses and mixing, aiming at simultaneously determine the flavor parameters and all the solar neutrino fluxes with a minimum set of theoretical priors. Since then more data have been accumulated by the solar neutrino experiments, and new non-solar neutrino experiments have provided a more accurate determination of the neutrino oscillation parameters. Thus in this work we present an update of our former analysis. In Sec. 2 we briefly summarize our methodology, data included and physical assumptions. In Sec. 3 we give the new reconstructed posterior probability distribution function for the eight normalization parameters of the solar neutrino fluxes, with and without the constraint imposed by the observed solar luminosity. In Sec. 4 we use the results of this analysis to statistically test to what degree the present solar neutrino data can discriminate between the two SSMs, and we estimate whether the present data are precise enough to provide useful information to the construction of the SSM. Finally

in Sec. 6 we summarize our conclusions.

2 Analysis framework

In the analysis of solar neutrino experiments we include the total rates from the radiochemical experiments Chlorine [26], Gallex/GNO [27] and SAGE [28]. For real-time experiments we include the results on electron scattering (ES) from the four phases in Super-Kamiokande: the 44 data points of the phase I (SK1) energy-zenith spectrum [29], the 33 data points of the full energy and day/night spectrum in phase II (SK2) [30], the 42 energy and day/night data points in phase III (SK3) [31], and the 24 data points of the energy spectrum and day-night asymmetry of the 1669-day of phase IV (SK4) [32]. The results of the three phases of SNO are included in terms of the parametrization given in their combined analysis [33] which amount to 7 data points. We also include the main set of the 740.7 days of Borexino Phase-1 data [34, 35] as well as their high-energy spectrum from 246 live days [36] and the 408 days of Borexino Phase-2 data [37]. Details of our Borexino Phase-2 data analysis which is totally novel in this article are presented in Appendix A. In the framework of three neutrino masses and mixing the expected values for these solar neutrino observables depend on the parameters Δm_{21}^2 , θ_{12} , and θ_{13} as well as on the normalizations of the eight solar fluxes.

Besides solar experiments, we also include the observed energy spectrum in KamLAND data sets DS-1 and DS-2 [38] with a total exposure of 3.49×10^{32} target-proton-year (2135 days), which in the framework of three neutrino mixing also yield information on the parameters Δm_{21}^2 , θ_{12} , and θ_{13} .

In addition, we include the information on θ_{13} obtained after marginalizing over $\Delta m_{3\ell}^2$, θ_{23} and δ_{CP} the results of all the other oscillation experiments considered in the NuFIT-2.0 analysis presented in Refs. [39–41]. In particular this accounts for Super-Kamiokande atmospheric neutrino data from phases SK1–4 [42] (with addition of the 1775 days of phase SK4 over their published results on phases SK1–3 [43]); the energy distribution of long baseline neutrinos from MINOS in both ν_μ and $\bar{\nu}_\mu$ disappearance with 10.71×10^{20} and 3.36×10^{20} pot, respectively, as well as from T2K in ν_μ disappearance [44] with 6.57×10^{20} pot; LBL appearance results from MINOS [45] with exposure 10.6×10^{20} (ν_e) and 3.3×10^{20} ($\bar{\nu}_e$) pot, and from T2K with 6.57×10^{20} pot (ν_e) [46]; reactor data from the finalized experiments CHOOZ [47] and Palo Verde [48] together with the spectrum from Double Chooz with 227.9 days live time [49], and the 621-day spectrum from Daya Bay [50], as well as the near and far rates observed at RENO with 800 days of data-taking [51].

In what follows, for convenience, we will use as normalization parameters for the solar fluxes the reduced quantities:

$$f_i = \frac{\Phi_i}{\Phi_i^{\text{ref}}} \quad (2.1)$$

with $i = \text{pp}, {}^7\text{Be}, \text{pep}, {}^{13}\text{N}, {}^{15}\text{O}, {}^{17}\text{F}, {}^8\text{B}$, and hep . The numerical values of Φ_i^{ref} are set to the predictions of the GS98 solar model as given in Ref. [10] and are listed in Table 1. With this, the theoretical predictions for the relevant observables (after marginalizing over Δm_{23}^2 , θ_{23} and δ_{CP}) depend on eleven parameters: the three relevant oscillation parameters

Flux	$\Phi_i^{\text{ref}} [\text{cm}^{-2} \text{s}^{-1}]$	$\alpha_i [\text{MeV}]$	β_i
pp	5.98×10^{10}	13.0987	9.186×10^{-1}
${}^7\text{Be}$	5.00×10^9	12.6008	7.388×10^{-2}
pep	1.44×10^8	11.9193	2.013×10^{-3}
${}^{13}\text{N}$	2.96×10^8	3.4577	1.200×10^{-3}
${}^{15}\text{O}$	2.23×10^8	21.570	5.641×10^{-3}
${}^{17}\text{F}$	5.52×10^6	2.3630	1.530×10^{-5}
${}^8\text{B}$	5.58×10^6	6.6305	4.339×10^{-5}
hep	8.04×10^3	3.7370	3.523×10^{-8}

Table 1. The reference neutrino flux Φ_i^{ref} used for normalization, the energy α_i provided to the star by nuclear fusion reactions associated with the i^{th} neutrino flux (taken from Ref. [53]), and the fractional contribution β_i of the i^{th} nuclear reaction to the total solar luminosity.

Δm_{21}^2 , θ_{12} , θ_{13} and the eight reduced solar fluxes f_i . With the data from the different data samples (D) and the theoretical predictions for them in terms of these parameters $\vec{\omega} = (\Delta m_{21}^2, \theta_{12}, \theta_{13}, f_{\text{pp}}, \dots, f_{\text{hep}})$ we build the corresponding likelihood function

$$\mathcal{L}(\text{D}|\vec{\omega}) = \frac{1}{N} \exp \left[-\frac{1}{2} \chi^2(\text{D}|\vec{\omega}) \right] \quad (2.2)$$

where N is a normalization factor. In Bayesian statistics our knowledge of $\vec{\omega}$ is summarized by the posterior probability distribution function (pdf)

$$p(\vec{\omega}|\text{D}, \mathcal{P}) = \frac{\mathcal{L}(\text{D}|\vec{\omega}) \pi(\vec{\omega}|\mathcal{P})}{\mathcal{Z}_{\mathcal{P}}} \quad (2.3)$$

where in the denominator we have introduced the so-called *evidence* $\mathcal{Z}_{\mathcal{P}}$

$$\mathcal{Z}_{\mathcal{P}} \equiv \text{Pr}(\text{D}|\mathcal{P}) = \int \mathcal{L}(\text{D}|\vec{\omega}') \pi(\vec{\omega}'|\mathcal{P}) d\vec{\omega}' \quad (2.4)$$

which gives the likelihood for the hypothesis (or model) \mathcal{P} to describe the data. Here $\pi(\vec{\omega}|\mathcal{P})$ is the prior probability density for the parameters in the hypothesis \mathcal{P} .

In our model-independent analysis we assume a uniform prior probability complemented by a set of constraints to ensure consistency in the pp-chain and CNO-cycle, as well as some relations from nuclear physics. Specifically, we impose the following restrictions:

- The fluxes must be positive:

$$\Phi_i \geq 0 \quad \Rightarrow \quad f_i \geq 0. \quad (2.5)$$

- The number of nuclear reactions terminating the pp-chain should not exceed the number of nuclear reactions which initiate it [52, 53]:

$$\begin{aligned}\Phi_{7\text{Be}} + \Phi_{8\text{B}} &\leq \Phi_{\text{pp}} + \Phi_{\text{pep}} \\ \Rightarrow \quad 8.49 \times 10^{-2} f_{7\text{Be}} + 9.95 \times 10^{-5} f_{8\text{B}} &\leq f_{\text{pp}} + 2.36 \times 10^{-3} f_{\text{pep}} .\end{aligned}\quad (2.6)$$

- The $^{14}\text{N}(p, \gamma)^{15}\text{O}$ reaction must be the slowest process in the main branch of the CNO-cycle [52]:

$$\Phi_{15\text{O}} \leq \Phi_{13\text{N}} \quad \Rightarrow \quad f_{15\text{O}} \leq 1.34 f_{13\text{N}} \quad (2.7)$$

and the CNO-II branch must be subdominant:

$$\Phi_{17\text{F}} \leq \Phi_{15\text{O}} \quad \Rightarrow \quad f_{17\text{F}} \leq 37 f_{15\text{O}} . \quad (2.8)$$

- The ratio of the pep neutrino flux to the pp neutrino flux is fixed to high accuracy because they have the same nuclear matrix element. We have constrained this ratio to match the average of the GS98 and AGSS09 values, with 1σ Gaussian uncertainty given by the difference between the values in the two models¹

$$\frac{f_{\text{pep}}}{f_{\text{pp}}} = 1.006 \pm 0.013 . \quad (2.9)$$

In this work we use MULTINEST [54–56], a Bayesian inference tool which, given the prior and the likelihood, calculates the evidence with an uncertainty estimate, and generates posterior samples from distributions that may contain multiple modes and pronounced (curving) degeneracies in high dimensions.

The number of independent fluxes is reduced when imposing the so-called “luminosity constraint”, *i.e.*, the requirement that the sum of the thermal energy generation rates associated with each of the solar neutrino fluxes coincides with the solar luminosity [57]:

$$\frac{L_{\odot}}{4\pi (\text{A.U.})^2} = \sum_{i=1}^8 \alpha_i \Phi_i . \quad (2.10)$$

Here the constant α_i is the energy provided to the star by the nuclear fusion reactions associated with the i^{th} neutrino flux; its numerical value is independent of details of the solar model to an accuracy of one part in 10^4 or better [53]. A detailed derivation of this equation and the numerical values of the coefficients α_i , which we reproduce for convenience in Table 1, is presented in Ref. [53]. In terms of the reduced fluxes Eq. (2.10) can be written as:

$$1 = \sum_{i=1}^8 \beta_i f_i \quad \text{with} \quad \beta_i \equiv \frac{\alpha_i \Phi_i^{\text{ref}}}{L_{\odot} / [4\pi (\text{A.U.})^2]} \quad (2.11)$$

where β_i is the fractional contribution to the total solar luminosity of the nuclear reactions responsible for the production of the Φ_i^{ref} neutrino flux, and $L_{\odot} / [4\pi (\text{A.U.})^2] = 8.5272 \times 10^{11} \text{ MeV cm}^{-2} \text{ s}^{-1}$ [53]. The analysis performed incorporating the priors in Eqs. (2.5–2.10)

¹We have verified that assuming a flat distribution over the 1σ uncertainty interval does not produce significant differences in the results of our analysis.

will be named “analysis with luminosity constraint”, $\mathcal{P} = L_\odot$, and for this case the prior probability distribution is:

$$\pi(\vec{\omega}'|L_\odot) = \begin{cases} \frac{1}{N} \exp \left[-\frac{(f_{\text{pep}}/f_{\text{pp}} - 1.006)^2}{2\sigma^2} \right] & \text{if Eqs. (2.5–2.8) and (2.10) are verified,} \\ 0 & \text{otherwise,} \end{cases} \quad (2.12)$$

where N is a normalization factor and $\sigma = 0.010$. When only Eqs. (2.5–2.9) are imposed we will speak of “analysis without luminosity constraint”, $\mathcal{P} = \mathcal{I}_\odot$, so:

$$\pi(\vec{\omega}'|\mathcal{I}_\odot) = \begin{cases} \frac{1}{N} \exp \left[-\frac{(f_{\text{pep}}/f_{\text{pp}} - 1.006)^2}{2\sigma^2} \right] & \text{if Eqs. (2.5–2.8) are verified,} \\ 0 & \text{otherwise.} \end{cases} \quad (2.13)$$

Let us notice that the conditions in Eqs. (2.5–2.8) and Eq. (2.10) are constraints on some linear combinations of the solar fluxes and they are model independent, *i.e.*, they do not impose any prior bias favoring either of the SSMs. Furthermore we have chosen to center the condition (2.9) at the average of the GS98 and AGSS09 values, with 1σ Gaussian uncertainty given by the difference between the values in the two models, to avoid the introduction of a bias towards one of the models. In the next sections we will comment on how our results are affected when this prior is centered about the GS98 or the AGSS09 prediction.

3 Determination of solar neutrino fluxes

Our results for the analysis with luminosity constraint are displayed in Fig. 1, where we show the marginalized one-dimensional probability distributions $p(f_i|\mathcal{D}, L_\odot)$ for the eight solar neutrino fluxes as well as the 90% and 99% CL two-dimensional allowed regions. The corresponding ranges at 1σ (and at the 99% CL in square brackets) on the oscillation parameters are:

$$\begin{aligned} \Delta m_{21}^2 &= 7.5 \pm 0.2 \left[{}^{+0.4}_{-0.5} \right] \times 10^{-5} \text{ eV}^2, \\ \sin^2 \theta_{12} &= 0.30 \pm 0.01 \left[{}^{+0.04}_{-0.03} \right], \\ \sin^2 \theta_{13} &= 0.022 \pm 0.001 \left[{}^{+0.002}_{-0.003} \right]. \end{aligned} \quad (3.1)$$

while for the solar neutrino fluxes we get:

$$\begin{aligned} f_{\text{pp}} &= 0.999^{+0.006}_{-0.005} \left[{}^{+0.012}_{-0.016} \right], & \Phi_{\text{pp}} &= 5.971^{+0.037}_{-0.033} \left[{}^{+0.073}_{-0.097} \right] \times 10^{10} \text{ cm}^{-2} \text{ s}^{-1}, \\ f_{7\text{Be}} &= 0.96^{+0.05}_{-0.04} \left[{}^{+0.12}_{-0.11} \right], & \Phi_{7\text{Be}} &= 4.80^{+0.24}_{-0.22} \left[{}^{+0.60}_{-0.57} \right] \times 10^9 \text{ cm}^{-2} \text{ s}^{-1}, \\ f_{\text{pep}} &= 1.005 \pm 0.009 \left[{}^{+0.019}_{-0.024} \right], & \Phi_{\text{pep}} &= 1.448 \pm 0.013 \left[{}^{+0.028}_{-0.034} \right] \times 10^8 \text{ cm}^{-2} \text{ s}^{-1}, \\ f_{13\text{N}} &= 1.7^{+2.9}_{-1.0} \left[{}^{+8.4}_{-1.6} \right], & \Phi_{13\text{N}} &\leq 13.7 \left[30.2 \right] \times 10^8 \text{ cm}^{-2} \text{ s}^{-1}, \\ f_{15\text{O}} &= 0.6^{+0.6}_{-0.4} \left[{}^{+2.0}_{-0.6} \right], & \Phi_{15\text{O}} &\leq 2.8 \left[5.8 \right] \times 10^8 \text{ cm}^{-2} \text{ s}^{-1}, \\ f_{17\text{F}} &\leq 15 \left[46 \right], & \Phi_{17\text{F}} &\leq 8.5 \left[25 \right] \times 10^7 \text{ cm}^{-2} \text{ s}^{-1}, \\ f_{8\text{B}} &= 0.92 \pm 0.02 \left[\pm 0.05 \right], & \Phi_{8\text{B}} &= 5.16^{+0.13}_{-0.09} \left[{}^{+0.30}_{-0.26} \right] \times 10^6 \text{ cm}^{-2} \text{ s}^{-1}, \\ f_{\text{hep}} &= 2.4^{+1.5}_{-1.2} \left[\leq 5.9 \right], & \Phi_{\text{hep}} &= 1.9^{+1.2}_{-0.9} \left[\leq 4.7 \right] \times 10^4 \text{ cm}^{-2} \text{ s}^{-1}. \end{aligned} \quad (3.2)$$

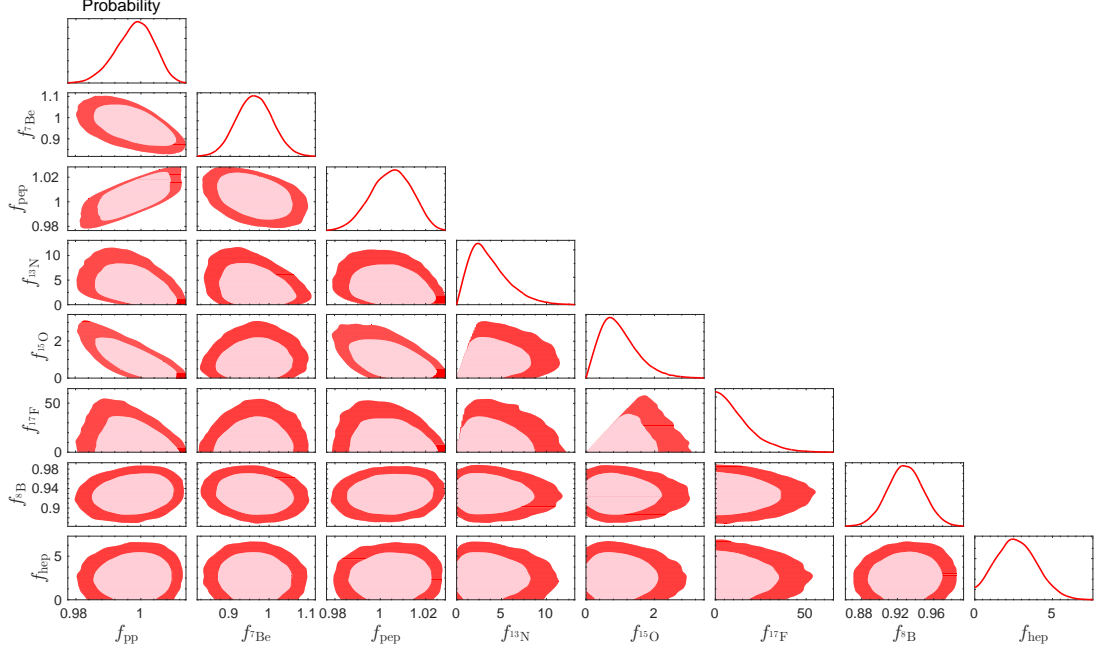


Figure 1. Constraints from our global analysis on the solar neutrino fluxes. The curves in the right-most panels show the marginalized one-dimensional probability distributions. The rest of the panels show the 90% and 99% CL two-dimensional credibility regions (see text for details).

We notice that with the exception of ^{17}F all other fluxes have a vanishing (or close to) probability for their corresponding $f = 0$. However, it is important to stress that for what concerns $f_{^{13}\text{N}}$ and $f_{^{15}\text{O}}$ this is mostly consequence of the inequalities in Eqs. (2.7) and (2.8), which effectively result into priors behaving as $\pi(f_i) \propto f_i$ for small f_i . For this reason the corresponding 1σ credible intervals for these fluxes, constructed as iso-posterior intervals and shown in the left column of Eq. (3.2), do not extend to $f_i = 0$ even though setting $f_{^{13}\text{N}} = f_{^{15}\text{O}} = f_{^{17}\text{F}} = 0$ gives a reasonable fit to the data. With this in mind, in the right column in Eq. (3.2) we have chosen to quote only the 1σ and 99%CL upper boundaries for the corresponding solar neutrino fluxes, rather than the complete allowed range.

As mentioned above we have checked the stability of the results under changes in the assumption of the Gaussian prior in Eq. (2.9). We find that if we center this prior at the GS98 prediction ($f_{\text{pep}}/f_{\text{pp}} = 1$) the best fit value for pep neutrinos is changed to $f_{\text{pep}} = 0.998$ ($\Phi_{\text{pep}} = 1.437 \times 10^8 \text{ cm}^{-2} \text{ s}^{-1}$), while if we center it at the AGSS09 prediction ($f_{\text{pep}}/f_{\text{pp}} = 1.013$) we get $f_{\text{pep}} = 1.012$ ($\Phi_{\text{pep}} = 1.457 \times 10^8 \text{ cm}^{-2} \text{ s}^{-1}$). All other fluxes are unaffected.

As seen in Fig. 1 the most important correlation appears between the pp and pep fluxes, as expected from the relation (2.9). The correlation between the pp (and pep) and ^7Be flux is directly dictated by the luminosity constraint (see comparison with Fig. 2). All these results imply the following share of the energy production between the pp-chain and the CNO-cycle

$$\frac{L_{\text{pp-chain}}}{L_{\odot}} = 0.991^{+0.005}_{-0.004} \left[{}^{+0.008}_{-0.013} \right] \iff \frac{L_{\text{CNO}}}{L_{\odot}} = 0.009^{+0.004}_{-0.005} \left[{}^{+0.013}_{-0.008} \right], \quad (3.3)$$

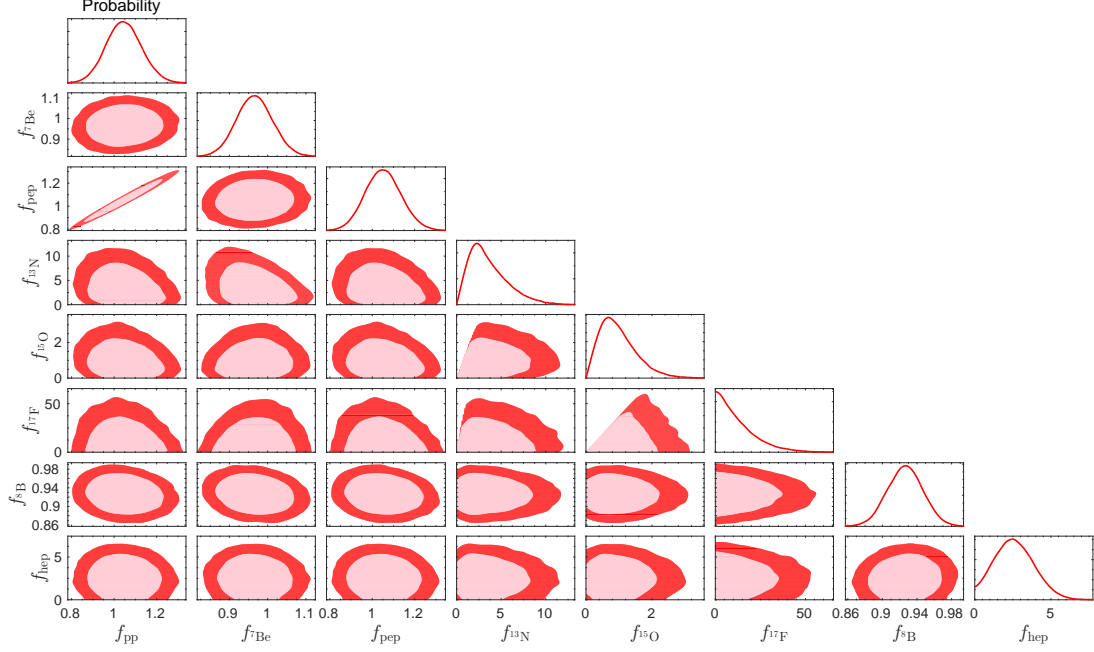


Figure 2. Same as Fig. 1 but without the luminosity constraint, Eq. (2.10).

in perfect agreement with the SSMs which predict $L_{\text{CNO}}/L_{\odot} \leq 1\%$ at the 3σ level. Note that the same comment as on the $f_{13\text{N}}$ and $f_{15\text{O}}$ fluxes applies to the total CNO luminosity, so we can understand the result in Eq. (3.3) effectively as an upper bound on the contribution of the CNO-cycle to the Sun Luminosity: $L_{\text{CNO}}/L_{\odot} \leq 2.2\%$ at 99% CL.

In order to check the consistency of our results we have performed the same analysis without imposing the luminosity constraint, Eq. (2.10). The corresponding results for $p(f_i|D, \mathbb{I}_{\odot})$ and the two-dimensional allowed regions are shown in Fig. 2. As expected, the pp flux is the most affected by the release of this constraint. This is so because the pp reaction gives the largest contribution to the solar energy production, as can be seen in Table 1. Hence, using the luminosity constraint only as an upper bound would imply that the pp flux cannot exceed its SSM prediction by more than 9%, while completely removing this constraint allows for a much larger pp flux. The pep flux is also severely affected due to its strong correlation with the pp flux, Eq. (2.9). On a smaller scale the CNO fluxes are also affected, mainly as an indirect effect due to the modified contribution of the pp and pep fluxes to the Gallium and Chlorine experiments, which leads to a change in the allowed CNO contribution to these experiments. Thus in this case we get:

$$\begin{aligned}
 f_{\text{pp}} &= 1.04 \pm 0.08 \left[{}^{+0.22}_{-0.20} \right], \\
 f_{7\text{Be}} &= 0.97^{+0.04}_{-0.05} \left[\pm 0.12 \right], \\
 f_{\text{pep}} &= 1.05 \pm 0.08 \left[{}^{+0.23}_{-0.20} \right], \\
 f_{13\text{N}} &= 1.7^{+2.8}_{-1.0} \left[{}^{+8.4}_{-1.6} \right], \\
 f_{15\text{O}} &= 0.6^{+0.7}_{-0.4} \left[\leq 2.6 \right], \\
 f_{17\text{F}} &\leq 15 \left[47 \right].
 \end{aligned} \tag{3.4}$$

$ \log(\text{odds}) $	odds	Interpolation
< 1.0	$\lesssim 3 : 1$	Inclusive
1.0	$\simeq 3 : 1$	Weak evidence
2.5	$\simeq 12 : 1$	Moderate evidence
5.0	$\simeq 150 : 1$	Strong evidence

Table 2. Values of Jeffrey’s scale used for the interpretation of model odds.

The determination of the ^8B and hep fluxes (as well as the oscillation parameters) is basically unaffected by the luminosity constraint.

Interestingly, the idea that the Sun shines because of nuclear fusion reactions can be tested accurately by comparing the observed photon luminosity of the Sun with the luminosity inferred from measurements of solar neutrino fluxes. We find that the energy production in the pp-chain and the CNO-cycle without imposing the luminosity constraint are given by:

$$\frac{L_{\text{pp-chain}}}{L_{\odot}} = 1.03^{+0.08}_{-0.07} \left[{}^{+0.21}_{-0.18} \right] \quad \text{and} \quad \frac{L_{\text{CNO}}}{L_{\odot}} = 0.008^{+0.005}_{-0.004} \left[{}^{+0.014}_{-0.007} \right]. \quad (3.5)$$

Comparing Eqs. (3.3) and (3.5) we see that the luminosity constraint has only a limited impact on the amount of energy produced in the CNO-cycle. However, as discussed above, the amount of energy in the pp-chain can now significantly exceed the total quantity allowed by the luminosity constraint. Altogether we find that the present value for the ratio of the neutrino-inferred solar luminosity, $L_{\odot}(\text{neutrino-inferred})$, to the photon luminosity L_{\odot} is:

$$\frac{L_{\odot}(\text{neutrino-inferred})}{L_{\odot}} = 1.04^{+0.07}_{-0.08} \left[{}^{+0.20}_{-0.18} \right]. \quad (3.6)$$

Thus we find that, at present, the neutrino-inferred luminosity perfectly agrees with the measured one, and this agreement is known with a 1σ uncertainty of 7%, which is a factor two smaller than the previous best determination [25].

4 Comparison with the Standard Solar Models

Next we compare the results of our determination of the solar fluxes with the expectations from the solar models, SSM=GS (for GS98) and SSM=AGS (for AGSS09). In order to do so we use the predictions $\langle f_i^{\text{SSM}} \rangle$ for the fluxes, the relative uncertainties σ_i^{SSM} and their correlations ρ_{ij}^{SSM} in both models as obtained from Refs. [10, 58]. The prior distribution $\pi(\vec{f}|\text{SSM})$ with maximum entropy (*i.e.*, minimum information) satisfying these constraints is a multivariate normal distribution, and this is what we assume in what follows. In Fig. 3 we show the marginalized one-dimensional probability distributions for the solar neutrino fluxes as determined by our analysis including the luminosity constraint, together with the corresponding prior distributions for the two SSMs.

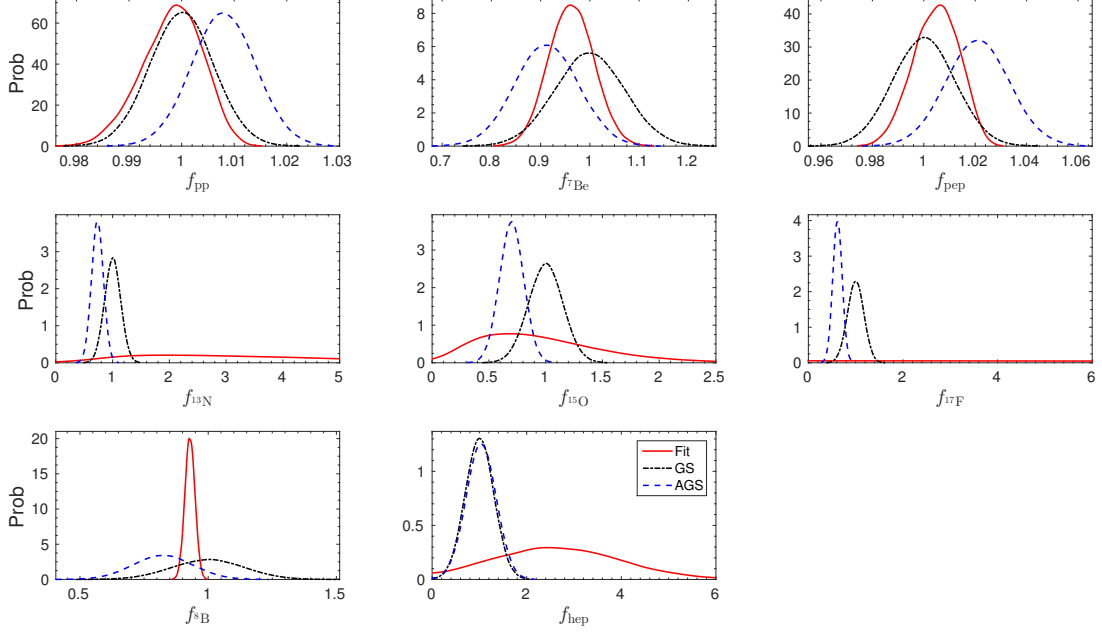


Figure 3. Marginalized one-dimensional probability distributions for the best determined solar fluxes in our analysis as compared to the predictions for the two SSMs in Ref. [10].

Comparison between the two models can be achieved by calculating the posterior odds, given data D , simply using Bayes' theorem

$$\frac{\Pr(\text{GS}|D)}{\Pr(\text{AGS}|D)} = \frac{\Pr(D|\text{GS}) \pi(\text{GS})}{\Pr(D|\text{AGS}) \pi(\text{AGS})} = \frac{\mathcal{Z}_{\text{GS}}}{\mathcal{Z}_{\text{AGS}}} \frac{\pi(\text{GS})}{\pi(\text{AGS})} \quad (4.1)$$

where we compute the evidences \mathcal{Z}_{SSM} as in Eq. (2.4) with the prior distributions for the f_i in each model and taking $\pi(\text{GS})/\pi(\text{AGS})$, the prior probability ratio for the two models, to be unity (this is, a priori both models are taken to be equally probable). The posterior odds can interpreted using the Jeffreys scale in Table 2.

Our calculation shows that $\log \mathcal{Z}_{\text{GS}}/\mathcal{Z}_{\text{AGS}} = 0.00 \pm 0.05$, meaning that the data has *absolutely* no preference to either model. Quantitatively this result is driven by the most precisely measured ^8B flux, which, as seen in Fig. 3, lies right in the middle of the predictions of GS98 and AGSS09. In what respects the possible discriminating power from the other precisely measured fluxes, in particular ^7Be and indirectly pp and pep, one must realize that within the SSMs the fluxes originating from the pp-chain are rather correlated among them; therefore, after the determination of the ^8B flux is imposed the posterior predictions of all the other pp-chain fluxes are also *pushed* towards the average of the two models, essentially making them indistinguishable with respect to measurements of these fluxes. In order to estimate how the correlations predicted by the SSM affect the comparison of the solar models, we define two new schemes GS' and AGS' where such correlations have been removed, *i.e.*, $\rho_{ij}^{\text{SSM}} = \delta_{ij}$. In this case we find $\log \mathcal{Z}_{\text{GS}'}/\mathcal{Z}_{\text{AGS}'} = 0.2 \pm 0.1$, meaning that even without the effect of the pp-chain correlations present data are unable to break the degeneracy between models implied by the ^8B measurement.

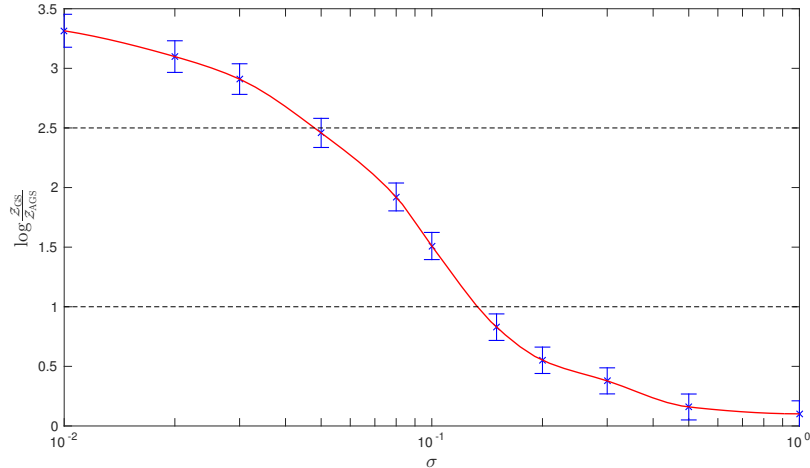


Figure 4. Bayes factor as a function of the assumed relative error on Φ_{CNO} . The bars give the numerical uncertainty of our calculations and the curve is a cubic interpolation. The dashed lines marks the limits for weak and moderate evidence of the Jeffreys scale, respectively.

On the other hand, the CNO fluxes are rather uncorrelated with the pp-chain fluxes, so even with the “democratic” ^8B flux result discussed above one could aim at discriminating between the solar models by measuring the CNO fluxes (also taking into account that their expectations strongly differ between the two models, as seen Fig. 3). To quantify this possibility we repeat our analysis including also an hypothetical future measurement of the total CNO flux, $\Phi_{\text{CNO}} = f_{13\text{N}}\Phi_{13\text{N}}^{\text{ref}} + f_{15\text{O}}\Phi_{15\text{O}}^{\text{ref}} + f_{17\text{F}}\Phi_{17\text{F}}^{\text{ref}}$, characterized by a given uncertainty σ_{CNO} and centered at the prior expectation of one of the models (for example the GS98 model, $\hat{\Phi}_{\text{CNO}} = 5.24 \times 10^8 \text{ cm}^{-2} \text{ s}^{-1}$). We plot in Fig. 4 the result of this exercise where we show the log of the Bayes factor as a function of the assumed relative error on Φ_{CNO} . From this figure we read that within the present model uncertainties a moderate evidence in favor of the model whose CNO fluxes have been assumed (GS98 in this case) can be achieved by a measurement of such fluxes with $\sigma_{\text{CNO}} = 5\%$ accuracy.

5 Generalizing/strengthening the solar models

Finally we make a first attempt to address whether the present data is precise enough to give relevant information which could be used as input for the construction of a more robust SSM. In order to do so we devise an analysis in which we naively generalize the SSM predictions by two parameters which are meant to characterize the best SSM from the point of view of the solar neutrino data.

First we notice that for most fluxes the theoretical correlations between the flux predictions of the solar models are pointing “in the same direction” as the difference between the mean of the predictions of the models. So it seems reasonable to make the solar models slightly more robust by letting the mean of the prediction vary continuously as

$$\hat{f}(t) = t\hat{f}_{\text{GS}} + (1-t)\hat{f}_{\text{AGS}}, \quad (5.1)$$

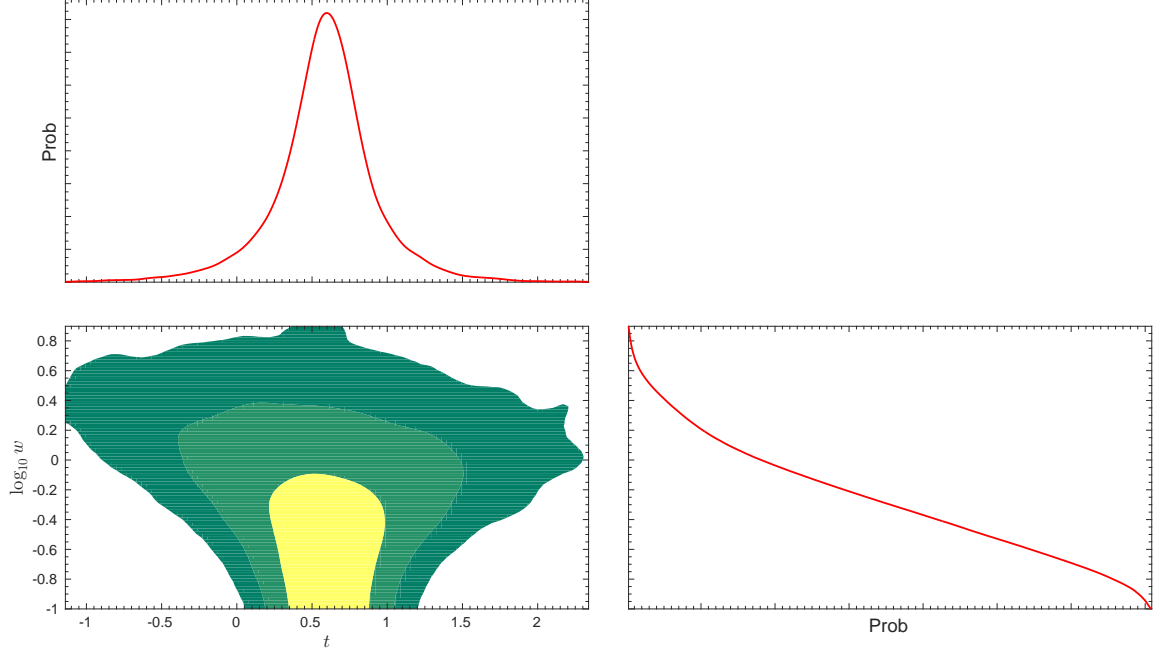


Figure 5. Results of the solar neutrino analysis for the generalized SSM. The lower left panel shows the two-dimensional iso-likelihood contours at 1σ , 2σ and 3σ in the plane (t, ω) . The upper left and lower right panels show the one-dimensional probability distributions for t and ω respectively.

where t now is an additional parameter. The AGS and GS solar models are recovered for $t = 0$ and $t = 1$, respectively. Then, by calculating the marginal likelihood of t , one can also evaluate the extent to which either of the two solar models is preferred or not compared to larger deviations (along the line of Eq. (5.1)). In addition, the Bayes factor calculated previously is simply the ratio of the marginal likelihood at $t = 0$ and $t = 1$, which serves as an additional check.

Second we consider how the inclusion of the neutrino data could affect “on average” the theoretical uncertainties of the model predictions. In order to do so we introduce a second parameter ω by which we rescale all σ_i^{SSM} .

We plot the results of this generalized-SSM analysis in Fig. 5 where we show the two-dimensional iso-likelihood contours for 1σ , 2σ and 3σ in the plane (t, ω) as well as the one-dimensional probability distributions for each parameter. From the upper panel we see that a model with $t \simeq 0.6$ is presently favored by the data, and provides a description which is clearly better than the limiting cases of the AGSS09 and GS98 models at $t = 0$ and $t = 1$ (characterized by rather similar probability as expected from the previous section). Also looking at the bi-dimensional region we see that this is more the case when allowing for smaller theoretical uncertainties than presently given in the SSM predictions, *i.e.*, the minimum likelihood lies at values of $\omega < 1$. The two-dimensional regions present a “funnel” shape at lower ω because σ_i^{SSM} becomes much smaller than σ_i^{FIT} and therefore the analysis becomes independent of ω . The fact that a better description of the neutrino data is obtained for a model with reduced theoretical uncertainties indicates that even with the

present neutrino data some refinement on the models can be obtained by including the results of the solar neutrino data as inputs in the model construction [59].

6 Summary and outlook

The pioneering proposal of using neutrinos to verify the source of the energy produced in the Sun has ended in the discovery of flavor conversion among solar neutrinos and in quantifying the contribution of the main mechanism of energy generation in the Sun. Further progress is needed to precisely answer some fundamental questions in solar evolution, such as (i) how much constrained are non-standard sources of energy, (ii) how much the CNO mechanism contributes to the solar energy generation, and (iii) what is the solution to the solar abundances problem.

In this work, we have updated the determination of solar model independent neutrino fluxes presented in Ref. [25] by taking into account the latest data from both solar and non-solar neutrino experiments. We have derived the best neutrino oscillation parameters and solar fluxes constraints using a Bayesian analysis with and without imposing nuclear physics as the only source of energy generation (luminosity constraint).

The precise measurement of the rate of ${}^7\text{Be}$ solar neutrinos by the Borexino experiment [34, 35] together with their first direct detection of pp neutrinos [37] and the very precise measurement of the mixing angle θ_{13} greatly contribute to answer the first question and constrain non-standard sources of energy, other than nuclear physics, as shown in Eq. (3.6). The uncertainty on the total luminosity due to nuclear physics derived from neutrino data has been reduced by a factor two and is now, for the first time, below 10%.

Present data cannot yet answer the second and third questions. The discovery of CNO neutrinos is within reach of the existing liquid scintillator detectors, if sufficient level of purification could be achieved. We have shown that present bounds on CNO neutrino fluxes are very close to the theoretical 3σ range, whether or not other sources of energy contribute to the energy generation. A discovery would not only verify the main mechanism of energy generation for bigger (or older) stars than our Sun, it would also help to solve the solar abundances problem. We have shown that a CNO flux measurement with $\sigma_{\text{CNO}} = 5\%$ uncertainty can lead to a moderate evidence in favor of one of the two alternative sets of solar abundances. Either the abundances are larger than what the most refined determinations indicate, or the opacities and stellar evolution codes have to be revisited to fit the precise helioseismology observations.

Acknowledgments

This work is supported by Spanish MINECO grants ESP2014-56003-R, FPA2011-29678, FPA2012-31880, FPA2012-34694 and FPA2013-46570, by the Severo Ochoa program SEV-2012-0249 of IFT, by the Maria de Maeztu program MDM-2014-0369 of ICCUB, and consolider-ingenio 2010 grant CSD-2008-0037, by CUR Generalitat de Catalunya grants 2014-SGR-104 and 2014-SGR-1458, by Generalitat Valenciana Prometeo grant II/2014/050,

by USA-NSF grant PHY-13-16617, and by EU grant FP7 ITN INVISIBLES (Marie Curie Actions PITN-GA-2011-289442).

A Borexino

Our analysis of the pp neutrino signal recently observed by Borexino is entirely based on the information provided in [37]. The set of operations which we have performed in order to gain confidence with such data can be broadly divided into two parts. First of all, we have focused solely on reproducing their fit, which involves extracting the information from the paper and ensuring that we can handle it properly. In this part we define:

$$N_b^{\text{th}}(\vec{\xi}) = N_b^{\text{sun}}(\vec{\xi}) + N_b^{\text{bkg}}(\vec{\xi}) \quad \text{with} \quad \begin{cases} N_b^{\text{sun}}(\vec{\xi}) = \sum_f N_{b,f}^{\text{sun}} (1 + \pi_f^{\text{sun}} \xi_f^{\text{sun}}), \\ N_b^{\text{bkg}}(\vec{\xi}) = \sum_i N_{b,i}^{\text{bkg}} (1 + \pi_i^{\text{bkg}} \xi_i^{\text{bkg}}) \end{cases} \quad (\text{A.1})$$

where $\vec{\xi}$ is a set of variables parametrizing the theoretical and systematic uncertainties. Here $b \in \{1, \dots, 158\}$ identifies the data bin, $f \in \{\text{pp}, {}^7\text{Be}, \text{pep}, \text{CNO}\}$ is the solar flux, and $i \in \{{}^{14}\text{C}, {}^{85}\text{Kr}, {}^{210}\text{Bi}, {}^{210}\text{Po}, {}^{214}\text{Pb}, \text{pile-up}\}$ labels the background component. Following Refs. [37, 60] we define the priors π_f^{sun} and π_i^{bkg} as follows:

$$\begin{aligned} \text{fixed: } & \pi_{\text{pep}}^{\text{sun}} = \pi_{\text{CNO}}^{\text{sun}} = \pi_{214\text{Pb}}^{\text{bkg}} = 0, \\ \text{constrained: } & \pi_{7\text{Be}}^{\text{sun}} = 2.3/48, \quad \pi_{14\text{C}}^{\text{bkg}} = 1/40, \quad \pi_{\text{pile-up}}^{\text{bkg}} = 7/321, \\ \text{free: } & \pi_{\text{pp}}^{\text{sun}} = \pi_{85\text{Kr}}^{\text{bkg}} = \pi_{210\text{Po}}^{\text{bkg}} = \pi_{210\text{Bi}}^{\text{bkg}} \rightarrow \infty. \end{aligned} \quad (\text{A.2})$$

We have extracted both the solar neutrino fluxes and the backgrounds from the upper panel of Fig. 3 of Ref. [37]. We have converted these spectra into absolute number of events for each bin b (for the solar flux and the background) by multiplying the given event rates (c.p.d. per 100 t per keV) by the total data-taking time ($T^{\text{run}} = 408$ days), the fiducial volume (75.47 t), and the specific bin energy size. We have verified that the sum of the different contributions agrees reasonably well (within the resolution of the figure) with the “best-fit prediction” shown as a black solid line in the figure. We have taken care to rescale the ${}^{14}\text{C}$ and the ${}^7\text{Be}$ spectra extracted from Ref. [37] by 40/39.8 and 48/46.2, respectively, to match the priors quoted in Sec. 3.4 of Ref. [60].

In order to test our ability to reproduce the Borexino fit, we have constructed a χ^2 function as follows:

$$\chi^2 = \min_{\vec{\xi}} \left\{ \sum_b \frac{[N_b^{\text{th}}(\vec{\xi}) - N_b^{\text{ex}}]^2}{N_b^{\text{ex}}} + \sum_f (\xi_f^{\text{sun}})^2 + \sum_i (\xi_i^{\text{bkg}})^2 \right\}. \quad (\text{A.3})$$

Here N_b^{ex} is the observed number of events for the bin b , which we have derived from the residuals ρ_b shown in the lower panel of Fig. 3. Note that, lacking the information on possible correlations among different bins, we have assumed that the experimental data are uncorrelated and that the statistical error is simply the square root of the number of

events, which implies $\sqrt{N_b^{\text{ex}}} = \rho_b/2 + \sqrt{(\rho_b/2)^2 + N_b^{\text{th}}}$. We have then performed a fit of the various spectra against the experimental data, and we have verified that the best-fit values and allowed ranges which we obtain (both solar fluxes and backgrounds) are in excellent agreement with those listed above Fig. 3. This proves that our simplified approach is credible and ensures a realistic determination of the solar flux normalizations, which is the main topic of this work.

The second step of our procedure requires embedding this fit into our global analysis in a consistent way, and making sure that its accuracy is not spoiled. To this aim, we now discard the solar spectra $N_b^{\text{sun}}(\vec{\xi})$ previously introduced in Eq. (A.1) and define instead:

$$N_b^{\text{th}}(\vec{\omega}, \vec{\xi}) = n_{\text{el}} T^{\text{run}} \sum_{\alpha} \int \frac{d\Phi_{\alpha}^{\text{det}}}{dE_{\nu}}(E_{\nu}|\vec{\omega}) \frac{d\sigma_{\alpha}}{dT_e}(E_{\nu}, T_e) R_b(T_e|\vec{\xi}) dE_{\nu} + N_b^{\text{bkg}}(\vec{\xi}). \quad (\text{A.4})$$

Note that the backgrounds $N_b^{\text{bkg}}(\vec{\xi})$ are the same as before. In Eq. (A.4) $\vec{\omega}$ describes both the neutrino oscillation parameters and the eight solar flux normalizations, n_{el} is the number of electron targets, $d\sigma_{\alpha}/dT_e$ is the elastic scattering differential cross-section for neutrinos of type $\alpha \in \{e, \mu, \tau\}$, and $d\Phi_{\alpha}^{\text{det}}/dE_{\nu}$ is the corresponding flux of solar neutrinos *at the detector* – hence it incorporates the neutrino oscillation probabilities. For comparison with the Borexino results we have used a three-neutrino oscillation model with values $\sin^2 \theta_{13} = 0.022$, $\sin^2 \theta_{13} = 0.304$ and $\Delta m_{21}^2 = 7.5 \times 10^{-5} \text{ eV}^2$ for the relevant parameters, and assumed the GS98 solar model.

The detector response function $R_b(T_e|\vec{\xi})$ depends on the *true* electron kinetic energy T_e as well as three new systematic variables ξ_{vol} , ξ_{scl} and ξ_{res} which we have included for completeness and consistency with the simulations of other experiments:

$$R_b(T_e|\vec{\xi}) = (1 + \pi_{\text{vol}} \xi_{\text{vol}}) \int_{T_b^{\text{min}}(1+\pi_{\text{scl}}^b \xi_{\text{scl}})}^{T_b^{\text{max}}(1+\pi_{\text{scl}}^b \xi_{\text{scl}})} \text{Gauss}[T_e - T', \sigma_T(1 + \pi_{\text{res}} \xi_{\text{res}})] dT'. \quad (\text{A.5})$$

Here $\text{Gauss}(x, \sigma) \equiv \exp[-x^2/2\sigma^2]/\sqrt{2\pi}\sigma$ is the normal distribution function, while T_b^{min} and T_b^{max} are the boundaries of the *reconstructed* electron kinetic energy T' in the bin b . We have assumed an energy resolution $\sigma_T/T_e = 5.5\%/\sqrt{T_e [\text{MeV}]}$, a fiducial volume uncertainty $\pi_{\text{vol}} = 2\%$, an energy scale uncertainty $\pi_{\text{scl}} = 1\%$, and an arbitrary energy resolution uncertainty $\pi_{\text{res}} = 5\%$, all uncorrelated between Borexino Phase I and Phase II.

As a first check, we have explicitly verified that our first-principle calculation of the solar flux contribution to the various bins matches quite accurately the $N_{b,f}^{\text{sun}}$ spectra extracted from Fig. 3 of Ref. [37]. We have then constructed a new χ^2 function for Borexino Phase II:

$$\chi^2(\vec{\omega}) = \min_{\vec{\xi}} \left\{ \sum_b \frac{[N_b^{\text{th}}(\vec{\omega}, \vec{\xi}) - N_b^{\text{ex}}]^2}{N_b^{\text{ex}}} + \sum_i (\xi_i^{\text{bkg}})^2 + \xi_{\text{vol}}^2 + \xi_{\text{scl}}^2 + \xi_{\text{res}}^2 \right\} \quad (\text{A.6})$$

and we have verified once more that our final fit (after combining it with the Borexino Phase I data to provide a prior for the ${}^7\text{Be}$ flux) still yields the correct best-fit values and allowed ranges for both the pp solar flux normalization and the Borexino backgrounds.

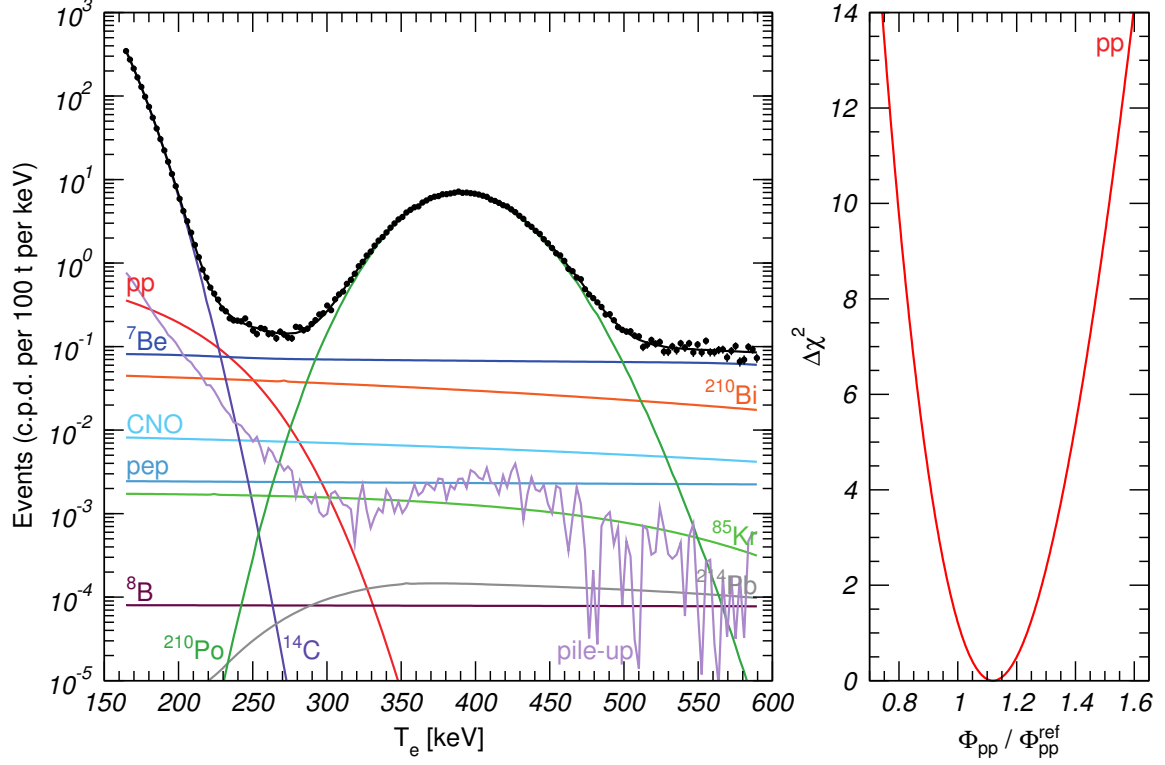


Figure 6. Spectrum for the best fit point of our spectral fit to the Borexino Phase II data in the energy region between 165–590 keV under the assumptions described in the Appendix (left), and $\Delta\chi^2$ as a function of the pp flux (right).

Thus we consider that our proposed goal, namely to embed Borexino pp data into our codes in a realistic and consistent way, has been accomplished.

In Fig. 6 we show the results of our analysis. Comparing the left panel with Fig. 3 of Ref. [37] we observe a very good agreement in the best fit determination of both solar fluxes and backgrounds, as mentioned above. In particular, the allowed range for Φ_{pp} is perfectly compatible with the value $\Phi_{pp} = (6.6 \pm 0.7) \times 10^{10} \text{ cm}^{-2} \text{ s}^{-1}$ quoted by the Borexino collaboration, as can be seen from the right panel where we plot the $\Delta\chi^2$.

References

- [1] H. A. Bethe, *Energy production in stars*, *Phys. Rev.* **55** (1939) 434–456.
- [2] J. N. Bahcall, *Neutrino Astrophysics*. Cambridge, UK: Univ. PR. (1989) 567p, 1989.
- [3] J. N. Bahcall and R. K. Ulrich, *Solar Models, Neutrino Experiments and Helioseismology*, *Rev. Mod. Phys.* **60** (1988) 297–372.
- [4] S. Turck-Chieze, S. Cahen, M. Casse and C. Doom, *Revisiting the standard solar model*, *Astrophys. J.* **335** (1988) 415–424.
- [5] J. N. Bahcall and M. H. Pinsonneault, *Standard solar models, with and without helium diffusion and the solar neutrino problem*, *Rev. Mod. Phys.* **64** (1992) 885–926.

- [6] J. N. Bahcall and M. H. Pinsonneault, *Solar models with helium and heavy element diffusion*, *Rev. Mod. Phys.* **67** (1995) 781–808, [[hep-ph/9505425](#)].
- [7] J. N. Bahcall, M. H. Pinsonneault and S. Basu, *Solar models: Current epoch and time dependences, neutrinos, and helioseismological properties*, *Astrophys. J.* **555** (2001) 990–1012, [[astro-ph/0010346](#)].
- [8] J. N. Bahcall, A. M. Serenelli and S. Basu, *New solar opacities, abundances, helioseismology, and neutrino fluxes*, *Astrophys. J.* **621** (2005) L85–L88, [[astro-ph/0412440](#)].
- [9] C. Pena-Garay and A. Serenelli, *Solar neutrinos and the solar composition problem*, [0811.2424](#).
- [10] A. M. Serenelli, W. C. Haxton and C. Pena-Garay, *Solar models with accretion. I. Application to the solar abundance problem*, *Astrophys. J.* **743** (2011) 24, [[1104.1639](#)].
- [11] J. N. Bahcall, *Solar neutrinos. I: Theoretical*, *Phys. Rev. Lett.* **12** (1964) 300–302.
- [12] J. N. Bahcall, N. A. Bahcall and G. Shaviv, *Present status of the theoretical predictions for the Cl-36 solar neutrino experiment*, *Phys. Rev. Lett.* **20** (1968) 1209–1212.
- [13] J. N. Bahcall and R. Davis, *Solar Neutrinos - a Scientific Puzzle*, *Science* **191** (1976) 264–267.
- [14] B. Pontecorvo, *Neutrino experiments and the problem of conservation of leptonic charge*, *Sov. Phys. JETP* **26** (1968) 984–988.
- [15] V. Gribov and B. Pontecorvo, *Neutrino astronomy and lepton charge*, *Phys. Lett.* **B28** (1969) 493.
- [16] L. Wolfenstein, *Neutrino Oscillations in Matter*, *Phys. Rev.* **D17** (1978) 2369–2374.
- [17] S. P. Mikheev and A. Yu. Smirnov, *Resonance Amplification of Oscillations in Matter and Spectroscopy of Solar Neutrinos*, *Sov. J. Nucl. Phys.* **42** (1985) 913–917. [*Yad. Fiz.* 42,1441(1985)].
- [18] J. N. Bahcall, S. Basu, M. Pinsonneault and A. M. Serenelli, *Helioseismological implications of recent solar abundance determinations*, *Astrophys. J.* **618** (2005) 1049–1056, [[astro-ph/0407060](#)].
- [19] N. Grevesse and A. J. Sauval, *Standard Solar Composition*, *Space Sci. Rev.* **85** (1998) 161–174.
- [20] M. Asplund, N. Grevesse and J. Sauval, *The Solar chemical composition*, *Nucl. Phys.* **A777** (2006) 1–4, [[astro-ph/0410214](#)]. [ASP Conf. Ser.336,25(2005)].
- [21] M. Asplund, N. Grevesse, A. J. Sauval and P. Scott, *The chemical composition of the Sun*, *Ann. Rev. Astron. Astrophys.* **47** (2009) 481–522, [[0909.0948](#)].
- [22] M. Castro, S. Vauclair and O. Richard, *Low abundances of heavy elements in the solar outer layers: comparisons of solar models with helioseismic inversions*, *Astron. & Astrophys.* **463** (Feb., 2007) 755–758, [[astro-ph/0611619](#)].
- [23] J. A. Guzik and K. Mussack, *Exploring Mass Loss, Low-Z Accretion, and Convective Overshoot in Solar Models to Mitigate the Solar Abundance Problem*, *Astrophys. J.* **713** (Apr., 2010) 1108–1119, [[1001.0648](#)].
- [24] A. Serenelli, S. Basu, J. W. Ferguson and M. Asplund, *New Solar Composition: The Problem With Solar Models Revisited*, *Astrophys. J.* **705** (2009) L123–L127, [[0909.2668](#)].

- [25] M. C. Gonzalez-Garcia, M. Maltoni and J. Salvado, *Direct determination of the solar neutrino fluxes from solar neutrino data*, *JHEP* **05** (2010) 072, [[0910.4584](#)].
- [26] B. T. Cleveland et al., *Measurement of the solar electron neutrino flux with the Homestake chlorine detector*, *Astrophys. J.* **496** (1998) 505–526.
- [27] F. Kaether, W. Hampel, G. Heusser, J. Kiko and T. Kirsten, *Reanalysis of the GALLEX solar neutrino flux and source experiments*, *Phys. Lett.* **B685** (2010) 47–54, [[1001.2731](#)].
- [28] SAGE collaboration, J. N. Abdurashitov et al., *Measurement of the solar neutrino capture rate with gallium metal. III: Results for the 2002–2007 data-taking period*, *Phys. Rev.* **C80** (2009) 015807, [[0901.2200](#)].
- [29] SUPER-KAMIOKANDE collaboration, J. Hosaka et al., *Solar neutrino measurements in Super-Kamiokande-I*, *Phys. Rev.* **D73** (2006) 112001, [[hep-ex/0508053](#)].
- [30] SUPER-KAMIOKANDE collaboration, J. Cravens et al., *Solar neutrino measurements in Super-Kamiokande-II*, *Phys. Rev.* **D78** (2008) 032002, [[0803.4312](#)].
- [31] SUPER-KAMIOKANDE collaboration, K. Abe et al., *Solar neutrino results in Super-Kamiokande-III*, *Phys. Rev.* **D83** (2011) 052010, [[1010.0118](#)].
- [32] Y. Koshio, “Solar Results from Super-Kamiokande.” Talk given at the *XXVI International Conference on Neutrino Physics and Astrophysics*, Boston, USA, June 2–7, 2014.
- [33] SNO collaboration, B. Aharmim et al., *Combined Analysis of all Three Phases of Solar Neutrino Data from the Sudbury Neutrino Observatory*, [1109.0763](#).
- [34] BOREXINO collaboration, G. Bellini et al., *Precision measurement of the ^7Be solar neutrino interaction rate in Borexino*, *Phys.Rev.Lett.* **107** (2011) 141302, [[1104.1816](#)].
- [35] BOREXINO collaboration, G. Bellini et al., *Final results of Borexino Phase-I on low energy solar neutrino spectroscopy*, *Phys. Rev.* **D89** (2014) 112007, [[1308.0443](#)].
- [36] BOREXINO collaboration, G. Bellini et al., *Measurement of the solar ^8B neutrino rate with a liquid scintillator target and 3 MeV energy threshold in the Borexino detector*, *Phys. Rev.* **D82** (2010) 033006, [[0808.2868](#)].
- [37] BOREXINO collaboration, G. Bellini et al., *Neutrinos from the primary proton-proton fusion process in the Sun*, *Nature* **512** (2014) 383–386.
- [38] KAMLAND collaboration, A. Gando et al., *Constraints on θ_{13} from A Three-Flavor Oscillation Analysis of Reactor Antineutrinos at KamLAND*, *Phys. Rev.* **D83** (2011) 052002, [[1009.4771](#)].
- [39] M. Gonzalez-Garcia, M. Maltoni and T. Schwetz, *Updated fit to three neutrino mixing: status of leptonic CP violation*, *JHEP* **1411** (2014) 052, [[1409.5439](#)].
- [40] J. Bergstrom, M. C. Gonzalez-Garcia, M. Maltoni and T. Schwetz, *Bayesian global analysis of neutrino oscillation data*, *JHEP* **09** (2015) 200, [[1507.04366](#)].
- [41] NuFIT webpage, <http://www.nu-fit.org>.
- [42] R. Wendell, “Atmospheric Results from Super-Kamiokande.” Talk given at the *XXVI International Conference on Neutrino Physics and Astrophysics*, Boston, USA, June 2–7, 2014.
- [43] SUPER-KAMIOKANDE COLLABORATION collaboration, R. Wendell et al., *Atmospheric neutrino oscillation analysis with sub-leading effects in Super-Kamiokande I, II, and III*, *Phys. Rev.* **D81** (2010) 092004, [[1002.3471](#)].

- [44] T2K collaboration, K. Abe et al., *Precise Measurement of the Neutrino Mixing Parameter θ_{23} from Muon Neutrino Disappearance in an Off-axis Beam*, *Phys. Rev. Lett.* **112** (2014) 181801, [[1403.1532](#)].
- [45] MINOS collaboration, P. Adamson et al., *Electron neutrino and antineutrino appearance in the full MINOS data sample*, *Phys. Rev. Lett.* (2013) , [[1301.4581](#)].
- [46] T2K collaboration, K. Abe et al., *Observation of Electron Neutrino Appearance in a Muon Neutrino Beam*, *Phys. Rev. Lett.* **112** (2014) 061802, [[1311.4750](#)].
- [47] CHOOZ collaboration, M. Apollonio et al., *Limits on Neutrino Oscillations from the CHOOZ Experiment*, *Phys. Lett.* **B466** (1999) 415–430, [[hep-ex/9907037](#)].
- [48] PALO VERDE collaboration, A. Piepke, *Final results from the Palo Verde neutrino oscillation experiment*, *Prog.Part.Nucl.Phys.* **48** (2002) 113–121.
- [49] DOUBLE CHOOZ collaboration, Y. Abe et al., *Reactor electron antineutrino disappearance in the Double Chooz experiment*, *Phys. Rev.* **D86** (2012) 052008, [[1207.6632](#)].
- [50] C. Zhang, “Recent Results From Daya Bay.” Talk given at the *XXVI International Conference on Neutrino Physics and Astrophysics*, Boston, USA, June 2–7, 2014.
- [51] S.-H. Seo, “New Results from RENO.” Talk given at the *XXVI International Conference on Neutrino Physics and Astrophysics*, Boston, USA, June 2–7, 2014.
- [52] J. N. Bahcall and P. I. Krastev, *How well do we (and will we) know solar neutrino fluxes and oscillation parameters?*, *Phys. Rev.* **D53** (1996) 4211–4225, [[hep-ph/9512378](#)].
- [53] J. N. Bahcall, *The Luminosity constraint on solar neutrino fluxes*, *Phys. Rev.* **C65** (2002) 025801, [[hep-ph/0108148](#)].
- [54] F. Feroz and M. Hobson, *Multimodal nested sampling: an efficient and robust alternative to MCMC methods for astronomical data analysis*, *Mon. Not. Roy. Astron. Soc.* **384** (2008) 449, [[0704.3704](#)].
- [55] F. Feroz, M. Hobson and M. Bridges, *MULTINEST: an efficient and robust Bayesian inference tool for cosmology and particle physics*, *Mon. Not. Roy. Astron. Soc.* **398** (2009) 1601–1614, [[0809.3437](#)].
- [56] F. Feroz, M. Hobson, E. Cameron and A. Pettitt, *Importance nested sampling and the MULTINEST algorithm*, [1306.2144](#).
- [57] M. Spiro and D. Vignaud, *Solar Model Independent Neutrino Oscillation Signals in the Forthcoming Solar Neutrino Experiments?*, *Phys. Lett.* **B242** (1990) 279–284. [[609\(1990\)](#)].
- [58] A. Serenelli. <http://www.mpa-garching.mpg.de/~aldos>.
- [59] N. Vinyoles, J. Bergstrom, M. Gonzalez-Garcia, M. Maltoni, C. Pena-Garay, A. Serenelli et al., *In preparation*, .
- [60] BOREXINO collaboration, O. Yu. Smirnov et al., *Measurement of neutrino flux from the primary proton-proton fusion process in the Sun with Borexino detector*, [1507.02432](#).